Chemistry of Metals and Alloys

Chem. Met. Alloys 7 (2014) 1-8
Ivan Franko National University of Lviv
www.chemetal-journal.org

Thermodynamics and crystal chemistry of the $RE_2MgNi_9H_{12-13}$ (*RE* = La and Nd) hydrides

Volodymyr YARTYS[1,2]*, Roman DENYS[1]

[1] *Department of Energy Systems, Institute for Energy Technology, Kjeller, NO 2027, Norway*
[2] *Department of Materials Science and Engineering, Norwegian University of Science and Technology, Trondheim NO 7491, Norway*
* *Corresponding author. Tel.: +47 45422065; fax: +47 63812905; e-mail: volodymyr.yartys@ife.no*

Dedicated to Evgen I. Gladyshevskii (1924-2012)

Received June 28, 2013; accepted June 26, 2014; available on-line November 10, 2014

Ternary *RE*-Mg-Ni intermetallics are promising negative electrode materials for high-energy/high-power Nickel-Metal Hydride (Ni-MH) batteries. These compounds belong to a family of hybrid layered structures (*AB*$_3$, *A*$_2$*B*$_7$ and *A*$_5$*B*$_{19}$; *A* = *RE*, Mg; *B* = Ni), composed of stacked Laves-type layers, $RE_{2-x}Mg_xNi_4$, and Haucke-type *RE*Ni$_5$ layers. In the present study structural and hydrogen storage properties of a new compound, Nd_2MgNi_9 ($PuNi_3$ type; *a* = 4.9783(1), *c* = 24.1865(6) Å), are reported and compared with those of the isostructural La_2MgNi_9 intermetallic. RE_2MgNi_9 (*RE* = La and Nd) were found to easily form hydrides containing 13 (La) or 12 (Nd) H/f.u. As for $La_2MgNi_9H_{13}$, formation of the $Nd_2MgNi_9H_{12}$ hydride proceeds via isotropic expansion of the unit cell (*a* = 5.3234(2), *c* = 26.506(2) Å; $\Delta V/V$ = 25.3 %). *In situ* neutron diffraction studies of the saturated deuterides $La_2MgNi_9D_{13}$ and $Nd_2MgNi_9D_{12}$, performed at SINQ, PSI, Switzerland, revealed: (a) nearly equal distribution of H atoms within the *RE*MgNi$_4$ and *RE*Ni$_5$ layers; (b) preferred filling of the Mg- and Ni-surrounded sites within the *RE*MgNi$_4$ layers; (c) local hydrogen ordering with the H-sublattice built from stacking of MgH_6 octahedra and NiH_4 tetrahedra, indicating directional metal–hydrogen bonding. In spite of the similarity of the crystal structures and hydrogenation capacities, $Nd_2MgNi_9H_{12}$ shows a significantly lower thermodynamic stability (ΔH_{des} = 29 kJ/mol H_2) than $La_2MgNi_9H_{13}$ (ΔH_{des} = 36 kJ/mol H_2).

Metal hydrides / Magnesium / Neodymium / Nickel / Powder neutron diffraction / Crystal structure / Hydrogen

Introduction

Rechargeable Nickel-Metal Hydride (Ni-MH) batteries are predominantly used in Hybrid Electric Vehicles (HEV). They offer significant advantages over the alternative secondary batteries, including excellent power densities, fast charge-discharge rates and long service life. The metal hydride electrode serves as a negative electrode in the NiMH battery. Commercial MH battery electrodes utilize *AB*$_5$-type rare earth-based alloys (*A* is a battery grade mixture of rare earths (La, Ce, Pr, Nd) and *B* is nickel or a mixture of various transition metals and aluminum (Ni, Co, Mn, Al)). R&D activities aimed at the improvement of the electrochemical discharge capacity of *AB*$_5$, 320 mA h/g, and decrease of the price of the metal hydride battery alloys, recently shifted focus towards studies of a new family of alloys composed of *AB*$_3$- and *A*$_2$*B*$_7$-type rare earth–magnesium-based intermetallics [1].

In our work at the Institute for Energy Technology in Norway we have studied various aspects of the metal-hydrogen systems formed during substitution of Mg for La in the $LaNi_3$ and La_2Ni_7 compounds [2-7]. These included:

(a) systematic studies of the influence of magnesium on the crystal structure and hydrogenation behavior of the $PuNi_3$-type $La_{3-x}Mg_xNi_9$ (x = 0-2) intermetallic alloys [4];

(b) neutron powder diffraction studies of the $La_2MgNi_9D_{13}$ deuteride, which witnessed local hydrogen ordering, with a hydrogen sublattice built from MgH_6 octahedra and NiH_4 tetrahedra [5];

(c) studies of the effect of the magnesium content and quenching rate on the phase structure and composition of a rapidly solidified La_2MgNi_9 metal hydride battery electrode alloy [6];

(d) studies of the effect of high-temperature annealing on the phase composition and electrochemical properties of a Co-free La_2MgNi_9 anode for Ni-metal hydride batteries [7];

(e) studies of the effect of La substitution by Nd on the phase-structural transformations in RE_2MgNi_9-H_2 systems [8]; and

(f) *in situ* neutron powder diffraction studies of the charge-discharge processes in metal hydride electrodes [9,10].

The present paper focuses on studies of the structure and thermodynamics of the Nd_2MgNi_9-based hydride. *In situ* neutron powder diffraction and Pressure-Composition-Temperature diagrams were studied, yielding crystal structure data and thermodynamics of the formation-decomposition of the saturated hydride $Nd_2MgNi_9H(D)_{12}$.

Experimental

Nd_2MgNi_9 alloy was prepared by a powder metallurgy route from a Nd_2Ni_9 alloy precursor and Mg powder (Alfa Aesar, 325 mesh, 99.8 %). The Nd_2Ni_9 alloy was arc-melted from the individual metals, Nd (99.98 %) and Ni (99.9 %), in a protective atmosphere of purified argon gas. The arc-melted pre-alloy Nd_2Ni_9 was crushed in a mortar and mixed with Mg. In order to obtain a homogeneous distribution of the components, the powder mixture was ball-milled in Ar atmosphere for one hour (Fritsch P6; 80 ml vial; balls/powder = 10/1; 150 rpm). The milled powder was pressed at 5 ton/cm^2 into pellets with a diameter of 8 mm. The pellets were placed into Ta containers, loaded into a sealed SS autoclave filled with argon gas (1 atm) and sintered at 950 °C for 6 h. Afterwards the alloy was annealed for 12 h at 800 °C and quenched into cold water. No evaporative loss of Mg occurred during the sintering/annealing treatment, as it was confirmed by measuring the mass of the samples.

Phase-structural analysis of the alloy was performed by X-ray powder diffraction using a Bruker D8 DISCOVER diffractometer with a Ge-monochromator (Cu $K\alpha_1$ radiation; λ = 1.5406 Å) and a LYNX-Eye detector. The experimental data were processed using Rietveld refinements and GSAS software [11].

The hydrogen absorption-desorption properties of the alloy were characterized using a Sievert's type system. The sample was activated in vacuum at 250 °C for 30 min, cooled to 20 °C and then charged with high-purity hydrogen gas (99.999 %). Pressure-composition-temperature (PCT) dependences of hydrogen absorption and desorption were measured on the activated sample at temperatures from 0 to 80 °C and H_2 pressures from 0.005 to 25 bar. In order to achieve activation, several complete hydrogen absorption-desorption cycles were performed prior to the PCT measurements to improve the kinetics of hydrogen exchange and to reach maximum hydrogen absorption capacities.

In situ neutron diffraction of the Nd_2MgNi_9-based deuteride was performed at the Spallation Neutron Source SINQ accommodated at the Paul Scherrer Institute, Villigen, Switzerland, using a high resolution powder diffractometer HRPT in the high intensity mode (λ = 1.494 Å, 2θ range 4.05-164.9°, step 0.05°). The deuteride was synthesized in a cylindrical stainless steel container (wall thickness 0.2 mm, d_{inner} = 6 mm), which was connected to a Sievert's type apparatus and used as the sample cell during the *in situ* NPD experiments. The sample was charged by deuterium (98 % purity) at room temperature and a pressure of 18 bar.

Results

Crystal structure of Nd_2MgNi_9

The X-ray phase analysis showed formation of a nearly single-phase alloy with the $PuNi_3$-type intermetallic compound Nd_2MgNi_9 as the main constituent (> 90 wt.%). Two minor secondary phases were observed in addition, $NdMgNi_4$ ($MgCu_4Sn$ type; space group *F*-43*m*; *a* = 7.0917(3) Å) and $NdNi_5$ ($CaCu_5$ type, space group *P*6/*mmm*; *a* = 4.9606(7), *c* = 3.9746(4) Å). The lattice parameters of the impurity phases are in good agreement with the reference data [12] and [13], respectively. Rietveld plots of the XRD pattern for the Nd_2MgNi_9 alloy are given in Fig. 1. Crystallographic data for the new compound Nd_2MgNi_9 are listed in Table 1. As expected, because of lanthanide contraction,

Table 1 Crystallographic data for Nd_2MgNi_9.
$PuNi_3$-type; space group *R*-3*m*; *a* = 4.9783(1), *c* = 24.1865(9) Å, *V* = 519.12(4) Å^3.

Atom	Wyckoff site	*x*/*a*	*y*/*b*	*z*/*c*	U_{iso}×100 (Å^2)	Occupancy
Nd1	3*a*	0	0	0	2.3(1)	1.0(–)
Nd2/Mg	6*c*	0	0	0.1467(2)	1.6(1)	0.525(9)/0.475(9)
Ni1	3*b*	0	0	½	0.3(1)	1.0(–)
Ni2	6*c*	0	0	0.3315(3)	0.3(1)	1.0(–)
Ni3	18*h*	0.4985(6)	–*x*	0.0825(2)	0.3(1)	1.0(–)

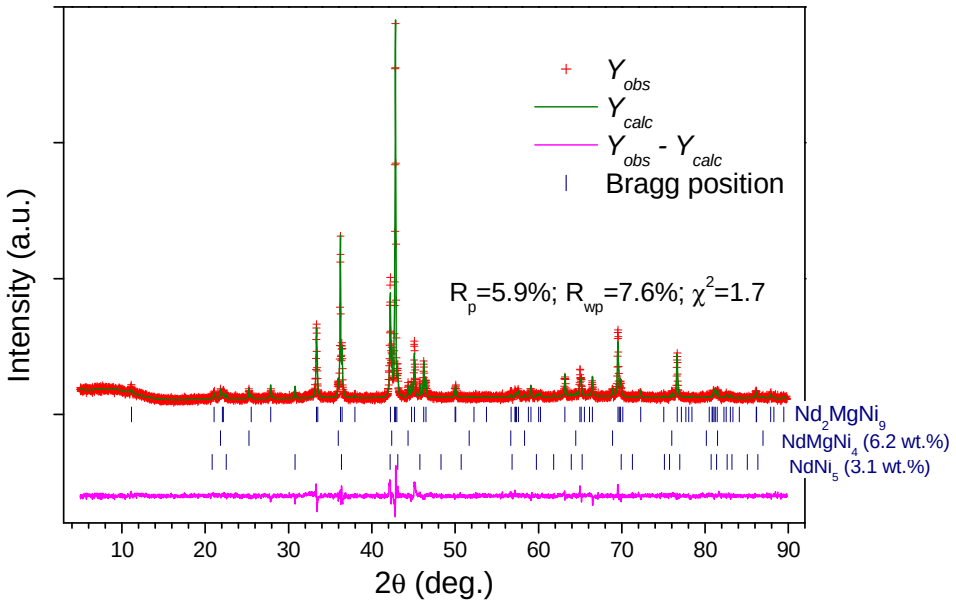

Fig. 1 XRD pattern of the Nd_2MgNi_9 alloy.

its unit cell dimensions (space group *R*-3*m*; *a* = 4.9783(1), *c* = 24.1865(9) Å; *V* = 519.12(4) Å^3) are slightly, by 0.5-1.1 %, lower than those of the isostructural intermetallic alloy La_2MgNi_9 (*a* = 5.0314(2); *c* = 24.302(1) Å; *V* = 532.79(3) Å^3) [5]. Similarly to other characterized hybrid structures built from the stacking of $CaCu_5$ and Laves type layers, Mg exclusively occupies the Laves type layer, substituting for half of the Nd atoms in the 6*c* site. In contrast, no Mg substitution for Nd takes place within the $CaCu_5$ layer (3*a* site), in agreement with earlier reports for (*RE*,Mg)Ni_x hybrid structures. The shortest interatomic distances (Å) in the structure of Nd_2MgNi_9 are: Nd1...(Nd2/Mg), 3.548(5) Å; (Nd2/Mg)...(Nd2/Mg), 3.032(3) Å; Nd1...Ni, 2.8746(1) Å; (Nd2/Mg)...Ni, 2.907(6) Å; Ni...Ni, 2.431(8) Å.

Thermodynamics and kinetics of the interactions in the Nd_2MgNi_9–H_2 system

After activation by fast heating in dynamic vacuum to ~250 °C, Nd_2MgNi_9 easily absorbs hydrogen already during the first hydrogenation. At room temperature, complete saturation of the alloy with hydrogen gas at a starting pressure of ~20 bar H_2 was reached within 15 min of interaction. The maximum hydrogen content reached under these conditions equals 12.2 H/f.u. (H/*M* = 1.0), which corresponds to 1.46 wt.% H. During the second hydrogenation cycle, the hydrogenation rate becomes nearly two times faster (at room temperature) and it further increases with increasing temperature (reducing the full hydrogenation time to ~2 min at 50-80 °C). The maximum hydrogenation capacity slightly increases at lower temperatures of hydrogenation, reaching 12.5 H/f.u. (1.48 wt.% H) at 0 °C and 20 bar H_2. Impurities give a minor contribution to the overall hydrogenation performance. Indeed, $NdNi_5$ remains non-hydrogenated, as it absorbs hydrogen at pressures exceeding 25 bar (room temperature) [10], which exceeds the pressure range used in the present work. On the other hand, at $P_{eq} \approx 1$ bar at 50 °C $NdMgNi_4$ forms a $NdMgNiH_4$ hydride containing 0.67 H/*M* [12]. As the content of $NdMgNi_4$ in the alloy, 6 wt.%, is very small, its effect on the overall absorption-desorption characteristics is marginal.

PCT measurements showed that $Nd_2MgNi_9H_{12}$ has a significantly lower thermodynamic stability than $La_2MgNi_9H_{13}$. Similarly to the La-based intermetallic, the Nd_2MgNi_9 compound shows a single pressure plateau type *P-C* diagram, corresponding to the transformation from an α solid solution of hydrogen in the intermetallic alloy to a β-hydride phase. However, as it is evident from the room temperature isotherms (Fig. 2), the equilibrium pressures of both hydrogen absorption and desorption in the Nd_2MgNi_9-H_2 system are by an order of magnitude higher than in the La_2MgNi_9-H_2 system. The equilibrium hydrogen desorption pressure changes from < 0.1 bar for the La_2MgNi_9-based hydride to > 1 bar for $Nd_2MgNi_9H_{12}$. Thermodynamic parameters of hydrogen desorption in the Nd_2MgNi_9-H_2 system were calculated from the van't Hoff dependencies of the midplateau pressure *versus* reciprocal temperature (Fig. 3). The enthalpy of hydrogen desorption for $Nd_2MgNi_9H_{12}$, 28.6(5) kJ/mol H_2, is lower than for $La_2MgNi_9H_{13}$, 35.9(3) kJ/mol H_2 [5].

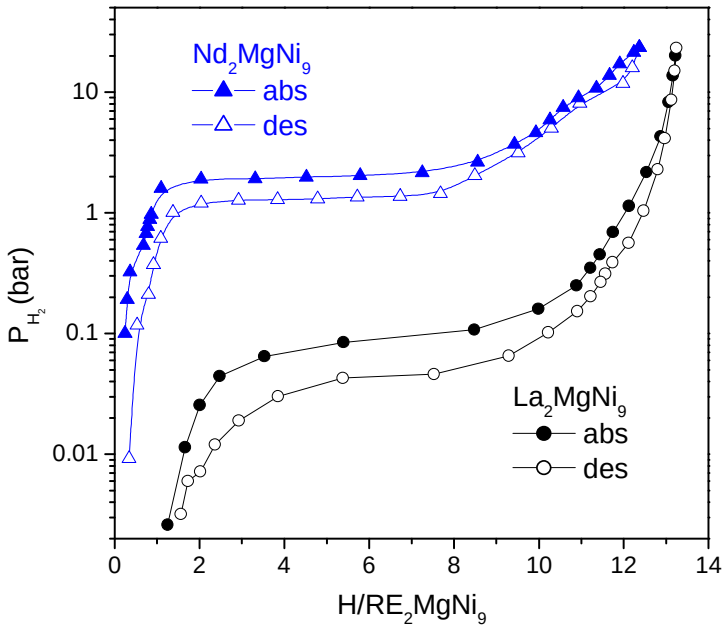

Fig. 2 *P-C* diagrams for the RE_2MgNi_9–H_2 systems with *RE* = La, Nd, measured at 20 °C.

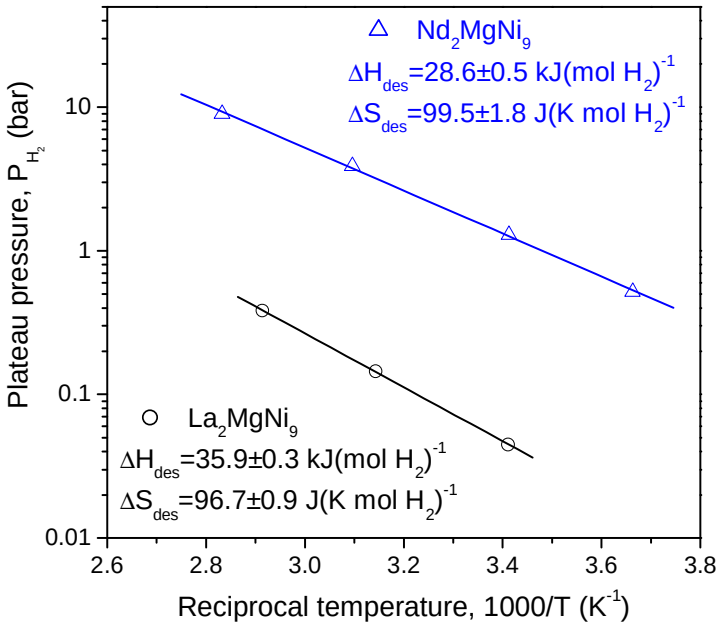

Fig. 3 Van't Hoff plots of hydrogen desorption in the RE_2MgNi_9-H_2 systems with *RE* = La, Nd.

Interestingly, the Nd_2MgNi_9-based β-hydride phase has an extremely broad homogeneity range with a H content changing from ~8 to more than 12 H/f.u. This unusual feature of the Nd_2MgNi_9–H_2 system is one of the subjects of our ongoing research.

Neutron powder diffraction study of the crystal structure of $Nd_2MgNi_9D_{12}$

The *in situ* NPD data for $Nd_2MgNi_9D_{12}$ were collected at a deuterium pressure of 18 bar and room temperature. Rietveld plots of the observed and calculated PND data are shown in Fig. 4. The phase composition of the deuterated alloy correlates well with that of the initial alloy (Fig. 1). In addition to the main, $Nd_2MgNi_9D_{12}$, deuteride phase, small amount of $NdMgNi_4$-based deuterides was also identified. The structure of the latter has previously been characterized by Guénée *et al.* [12] (space group $Pmn2_1$; a = 5.0767(2), b = 5.4743(2), c = 7.3792(3) Å), and was used as a model in our Rietveld refinements. As was already mentioned, the

intermetallic $NdNi_5$ does not form a hydride under the conditions applied in the present study. The structural data obtained for the $Nd_2MgNi_9D_{12}$ alloy are presented in Table 2. Similarly to $La_2MgNi_9H_{13}$ [5], formation of the $Nd_2MgNi_9H_{12}$ hydride proceeds via isotropic expansion of the unit cell ($\Delta a/a$ = 6.9 %, $\Delta c/c$ = 9.6 %, $\Delta V/V$ = 25.3 %).

D atoms partially occupy six types of interstitial position in both Laves and $CaCu_5$-type slabs. The volumetric expansion of these slabs is very similar; ΔV_{NdNi_5} = 25.9 %, ΔV_{NdMgNi_4} = 24.7 %. Three occupied D-sites (D1, D2 and D4) are located within the $NdNi_5$ slabs, while three other sites (D5, D6 and D8) are within the $NdMgNi_4$ slabs. From the overall stoichiometry of 12 D/f.u. Nd_2MgNi_9, 6.3(1) D are located inside the $NdNi_5$ slabs and 5.6(2) D fill the $NdMgNi_4$ slabs. The calculated D content, $Nd_2MgNi_9D_{11.9(3)}$ ($NdNi_5D_{6.3(1)}$ + $NdMgNi_4D_{5.6(2)}$), agrees within the uncertainty with the value of 12.1(1) D/f.u. obtained from volumetric measurements during the synthesis of the deuteride.

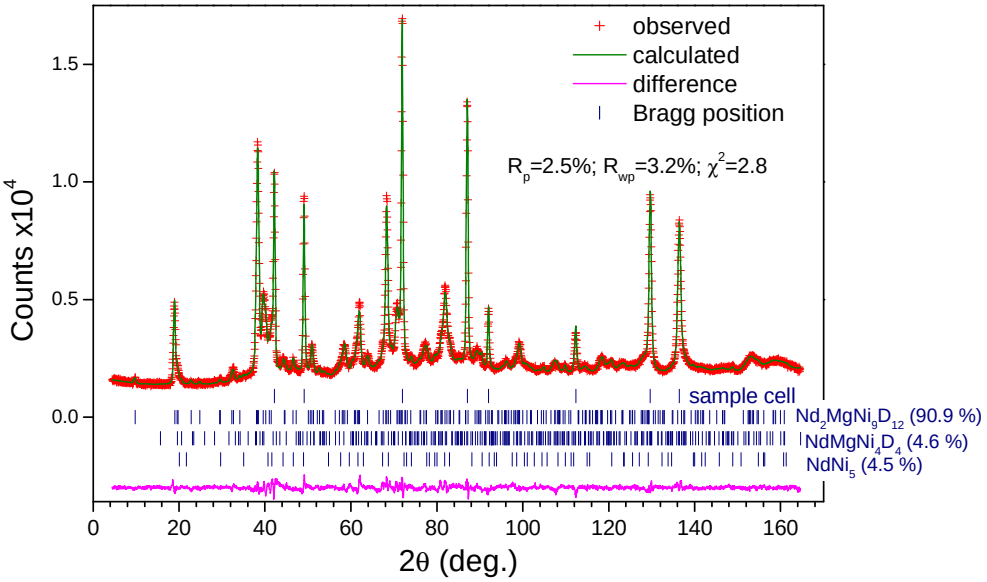

Fig. 4 *In situ* powder neutron diffraction pattern of the $Nd_2MgNi_9D_{12}$deuteride (300 K; 18 bar D_2).

Table 2 Crystallographic data for $Nd_2MgNi_9D_{12}$ from Rietveld refinements of *in situ* NPD data (300 K, 18 bar D_2). Space group *R*-3*m*; *a* = 5.3234(2), *c* = 26.506(2) Å, *V* = 650.50(6) Å^3.

Atom	Wyckoff site	*x*/*a*	*y*/*b*	*z*/*c*	U_{iso}×100 (Å^2)	Occupancy
Nd1	3*a*	0	0	0	0.6(2)	1.0(–)
Nd2/Mg	6*c*	0	0	0.1411(4)	2.2(2)	0.5/0.5(–)
Ni1	3*b*	0	0	½	2.6(2)	1.0(–)
Ni2	6*c*	0	0	0.3276(2)	1.2(1)	1.0(–)
Ni3	18*h*	0.4968(4)	–*x*	0.0829(1)	1.06(6)	1.0(–)
D1 [a]	36*i*	0.553(3)	0.560(3)	0.0180(4)	2.3(1)	0.242(5)
D2	6*c*	0	0	0.3876(6)	=U_{iso}(D1)	0.32(1)
D3 [b]	18*h*	0.157	–*x*	0.073	–	vacant
D4	18*h*	0.839(2)	–*x*	0.0690(6)	=U_{iso}(D1)	0.46(1)
D5	18*h*	0.499(1)	–*x*	0.1482(3)	=U_{iso}(D1)	0.465(8)
D6 [c]	18*h*	0.833(2)	–*x*	0.0977(7)	=U_{iso}(D1)	0.35(1)
D7 [b]	6*c*	0	0	0.235	–	vacant
D8	6*c*	0	0	0.4403(6)	=U_{iso}(D1)	0.35(2)
Calculated D-content:		11.9(3) D/f.u. (volumetric data 12.1(1) D/f.u.)				
R-values:		R_p = 2.5 %; R_{wp} = 3.3 %; R_{F^2} = 2.8 %; χ^2 = 2.94				

Notes: Labeling of D atoms adopted from [5].
[a] D1 is located in a 36*i* site (D1–D1 = 0.50(4) Å) rather than in a18*h* site as in the structure of $La_2MgNi_9D_{13}$.
[b] D3 and D7 are vacant in the structure of $Nd_2MgNi_9D_{12}$ but are occupied by D atoms in $La_2MgNi_9D_{13}$.
[c] D6 differs from that in the structure of $La_2MgNi_9D_{13}$; D is located in a $MgNi_2$ triangular face.

D atoms fill three types of tetrahedral interstice (D1: $NdNi_3$; D2 and D8: Ni_4; D4: Nd_2Ni_2). Furthermore, two D sites, D5 and D6, are located at the center of trigonal bipyramids, $(Nd2/Mg)_3Ni_2$ and $Nd1(Nd2/Mg)_2Ni_2$, and have triangular coordination $MgNi_2$. The conclusion stating such unusual coordination is based on the analysis of the distances between the metal atoms and deuterium positions. The mixed Nd2/Mg site is randomly occupied by Mg and Nd atoms in the ratio 50/50. The D5 and D6 sites are partially filled by D atoms with occupancies ≤ 50 %. The distances from the Nd2/Mg 6*c* site to the D5 and D6 sites are 1.91(1) and 1.97(2) Å, respectively. Apparently, both values are too short if the metal site is occupied by a large Nd atom (r_{Nd} = 1.82 Å); in contrast, they are in the same range as the Mg–D bond lengths in the structures of the α- and γ-MgD_2 binary hydrides, 1.9-2.0 Å [14]. Thus, D5 and D6 positions can only be occupied in the case when they have Mg atoms (r_{Mg} = 1.60 Å) in their nearest surrounding. The minimum distance between Nd and D atoms in the structure is 2.3 Å, while the Ni−D distances are within the range from 1.51 to 1.76 Å.

A comparison of the metal-metal distances in the structures of the initial compound and its hydride is given in Table 3; these distances quite significantly, by 8 % in average, increase on hydrogenation. The most pronounced expansion is observed in the coordination sphere of the Ni3 atoms.

Discussion and conclusions

Hydrogenation properties

The hydrogen sorption capacities, 12.2 and 13.3 H/f.u. RE_2MgNi_9 (*RE* = Nd and La) at 20 bar, are very close at RT. The single plateau behavior observed for the absorption-desorption isotherms corresponds to the formation of one hydride phase. The lower stability (higher formation/decomposition pressures) of the Nd_2MgNi_9-based hydride can be explained by the smaller unit cell volume, which is by 2.7 % smaller than that of $La_2MgNi_9H_{13}$. A similar correlation between the unit cell volume of the intermetallic alloy and the thermodynamic stability of the hydride is a well-documented feature for $RENi_5H_x$ hydrides (see *e.g.* [13]) and was also recently observed for a series of hydrogenated Mg-containing $La_{3-x}Mg_xNi_9$ (x = 0-2) alloys [4]; here changing of the Mg/La ratio in the $La_{3-x}Mg_xNi_9$ compound allows achieving a huge variation of the thermal stability of the hydrides. From the present study it can be concluded that partial substitution of Nd for La in the La_2MgNi_9 alloy will make it possible to optimize the hydrogenation-dehydrogenation behavior and to increase the rate of hydrogen exchange, allowing improvement of the electrochemical performance as negative electrodes for Ni-MH batteries.

Structural similarities between the hydrides

The formation of hydrides is accompanied by isotropic volumetric expansion. $RE_2MgNi_9D_{12-13}$ are formed by filling of existing interstitial sites, similarly to $CaCu_5$-type and Laves type hydrides. Detailed analysis of the metal-hydrogen coordination in the structures of $Nd_2MgNi_9D_{12}$ and $La_2MgNi_9D_{13}$ showed the presence of local hydrogen ordering around Mg and Ni atoms.

In situ neutron diffraction studies of the saturated deuterides revealed:
(a) a nearly equal distribution of H atoms within the $REMgNi_4$ and $RENi_5$ layers;
(b) preferred filling by hydrogen of Mg- and Ni-surrounded sites within the $REMgNi_4$ layers, triangles [$MgNi_2$] and tetrahedra [Ni_4].

Analysis of the neutron scattering data indicates that local hydrogen ordering takes place in the hydride, with the hydrogen sublattice being built from MgH_6 octahedra and NiH_4 tetrahedra (see Fig. 5).

Table 3 Metal–metal distances in the structures of Nd_2MgNi_9 and $Nd_2MgNi_9D_{12}$.

	Initial compound a = 4.9783(1) Å c = 24.1867(9) Å	Deuteride a = 5.3234(2) Å c = 24.506(2) Å	Change on hydrogenation $\Delta a/a$ = 6.9 % $\Delta c/c$ = 9.6 %
Nd1...2 Nd2/Mg	3.546(5)	3.739(9)	+5.4 %
Nd1...6 Ni2	2.8746(1)	3.0773(3)	+7.1 %
Nd1...12 Ni3	3.190(3)	3.451(2)	+8.2 %
Nd2/Mg...3 Nd2/Mg	3.034(3)	3.360(8)	+10.7 %
Nd2/Mg...3 Ni1	2.9149(8)	3.147(2)	+8.0 %
Nd2/Mg...6 Ni3	2.933(4)	3.077(5)	+4.9 %
Nd2/Mg...3 Ni3	2.910(6)	3.295(8)	+13.2 %
Ni1...6 Ni3	2.485(5)	2.684(4)	+8.0 %
Ni2...3 Ni3	2.487(7)	2.792(5)	+12.3 %
Ni2...3 Ni3	2.430(8)	2.575(6)	+6.0 %
Ni3...2 Ni3	2.513(9)	2.713(7)	+8.0 %
Ni3...2 Ni3	2.465(9)	2.611(7)	+5.9 %

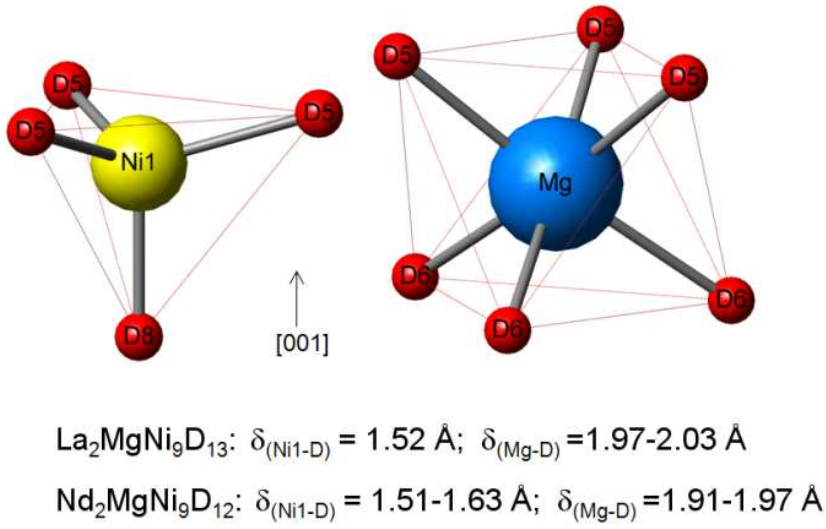

Fig. 5 Local hydrogen ordering around Mg and Ni in the structures of $La_2MgNi_9D_{13}$ and $Nd_2MgNi_9D_{12}$. An octahedron MgD_6 and a tetrahedron NiD_4 are shown.

Such local hydrogen ordering within the H-sublattice was first observed in the structure of $La_2MgNi_9H_{13}$ deuteride. Even if the number of hydrogen-filled sites in the Nd-containing hydride, 6, is lower than in $La_2MgNi_9H_{13}$, 8, this does not change the local ordering of hydrogen in the structures. The Mg–H and Ni–H distances are very close to each other in both structures.

The stacking of MgH_6 octahedra and NiH_4 tetrahedra stabilizes the structures and manifests directional bonding between the metal (Mg and Ni) and hydrogen atoms.

Finally, the coordination chemistry of intermetallic hydrides is based on the analysis of the coordination polyhedra of the atoms of smaller size (hydrogen) and the metal atoms in the structures. This concept allows finding interrelations between the structure and properties and optimizing the search for advanced hydrogen storage materials with improved performance. A similar concept was proposed at Lviv University more than 50 years ago by Prof. E.I. Gladyshevskii and was adopted to describe the crystal chemistry of silicides and germanides [15]. One of the authors of the present contribution (VAY) had the pleasure and privilege to start his research as a student supervised by Evgen Ivanovych. The unlimited energy of Prof. E.I. Gladyshevskii, his scientific courage in challenging new research topics, together with a broad competence in materials science and crystal chemistry and personal charisma will be remembered and respected for many years ahead by the international research community and by Lviv school of crystal chemistry of the intermetallic alloys.

References

[1] Y. Liu, Y. Cao, L. Huang, M. Gao, H. Pan, *J. Alloys Compd.* 509(3) (2011) 675-686.
[2] R.V. Denys, A.B. Riabov, V.A. Yartys, R.G. Delaplane, M. Sato, *J. Alloys Compd.* 446-447 (2007) 166-172.
[3] R.V. Denys, A.B. Riabov, V.A. Yartys, M. Sato, R.G. Delaplane, *J. Solid State Chem.* 181(4) (2008) 812-821.
[4] R.V. Denys, V.A. Yartys, *J. Alloys Compd.* 509 (Suppl. 2) (2011) S540-S548.
[5] R.V. Denys, V.A. Yartys, C.J. Webb. *Inorg. Chem.* 51 (2012) 4231-4238.
[6] C.C. Nwakwuo, T. Holm, R.V. Denys, W. Hu, J.P. Maehlen, J.K. Solberg, V.A. Yartys, *J. Alloys Compd.* 555 (2013) 201-208.
[7] W. Hu, R.V. Denys, C.C. Nwakwuo, T. Holm, J.P. Maehlen, J.K. Solberg, V.A. Yartys, *Electrochim. Acta* 96 (2013) 27-33.
[8] R.V. Denys, V.A. Yartys, to be published in *J. Phys. Chem. C.*
[9] A.B. Riabov, M. Latroche, F. Cuevas, R.V. Denys, Weikang Hu, V.A. Yartys, *Abstr. Int. Symp. Metal-Hydrogen Systems* (*MH2012*), Kyoto, Japan, 2012, p. 421.
[10] M. Latroche, F. Cuevas, W.-K. Hu, D. Sheptyakov, R.V. Denys, V.A. Yartys, *J. Phys. Chem. C*, 118 (2014) 12162–12169.
[11] A.C. Larson, R.B.V. Dreele, *General Structure Analysis System (GSAS)*, Los Alamos National Laboratory Report LAUR, 2000, pp. 86-748.

[12] L. Guénée, V. Favre-Nicolin, K. Yvon, *J. Alloys Compd*. 348 (2003) 129-137.
[13] H. Senoh, N. Takeichi, H.T. Takeshita, H. Tanaka, T. Kiyobayashi, N. Kuriyama, *Mater. Trans.* 44(9) (2003) 1663-1666.
[14] M. Bortz, B. Bertheville, G. Bottger, K. Yvon, *J. Alloys Compd.* 287 (1999) L4-L6.
[15] E.I. Gladyshevskii, *Crystal Chemistry of Silicides and Germanides*, Metallurgiya, Moscow, 1971 (in Russian).